Journal of Nano- and Electronic Physics
Vol. **7** No 3, 03021(6pp) (2015)

Журнал нано- та електронної фізики
Том **7** № 3, 03021(6cc) (2015)

Structure and Optical Properties of Nickel-Cobalt Ferrites Obtained by the Sol-gel Method with Participation of Auto-combustion

V.S. Bushkova*

Vasyl Stefanyk Pre-Carpathian National University, 57, Shevchenko Str., 76025 Ivano-Frankivsk, Ukraine

(Received 25 June 2015; published online 20 October 2015)

In this work, ferrite nickel-cobalt powders were synthesized using sol-gel technology with participation of auto-combustion. After completing the auto-combustion process, only one phase, which corresponds to the cubic structure of spinel space group $Fd3m$, was obtained. It was found that the average size of coherent scattering regions does not exceed 62 nm. The dependences of the lattice parameter, X-ray density and specific surface area of the ferrite powders on the nickel content were found. It was shown that at substitution of cobalt cations by nickel cations, the latter occupy only B positions, thus displacing a part of Fe^{3+} into A positions. The optical properties of the powders depending on the degree of substitution of cobalt cations by nickel cations are studied. As a result of analysis of the absorption spectra, it is revealed that the allowed direct transition of electrons from the valence band to the conduction band is inherent for all investigated powders. It was shown that the optical band gap increases with increasing concentration of nickel cations in the composition of ferrites.

Keywords: Sol-gel technology, Nickel-cobalt ferrite, Lattice parameter, Cationic distribution, Absorption coefficient, Optical band gap.

PACS numbers: 82.45.Yz, 82.47.Uv, 71.20.Tx

1. INTRODUCTION

Hundreds of various brands of ferrites, which differ in chemical composition, crystal structure, magnetic, optical and other properties, are known today. Besides single-component ferrites, two- and multicomponent ferrites with continuously expanding areas of use have found a wide application. The majority of ferrites possess magnetic properties even at high temperatures; moreover, they have high resistivity and low dielectric losses due to the absence of eddy currents [1, 2].

Ferrites with the spinel structure, whose chemical formula is $MeFe_2O_4$, where Me are the cations of Fe, Co, Ni, etc., are very important group of magnetic materials. They include a wide spectrum of applications, starting from low-wave to microwave technology [3-5].

The unit cell of spinel represents a cube with an edge of $a \approx 8.5$ Å. In general, the unit cell consists of 8 molecules, i.e. of 32 oxygen ions, 16 iron ions and 8 bivalent metal ions. Oxygen ions form the face-centered cubic cell. The crystal structure of spinel ferrite is composed of two types of cavities: tetrahedral and octahedral, which are formed of four and six oxygen ions, respectively. Tetrahedral cavities are accepted to be called the $8a$ position or non-equivalent A-sublattice, and octahedral ones – $16d$ position or B-sublattice. Taking into account this fact, the unit cubic lattice contains 64 tetrahedral and 32 octahedral cavities, among which only 8 tetrahedral and 16 octahedral are occupied by the metal ions, therefore, there is a real possibility for different deviations from the perfect spinel structure.

The inverse spinel ferrites are especially interesting from the practical point of view among spinel ferrites due to high crystallographic anisotropy, high saturation magnetization and unique magnetic structure [6]. Cobalt ferrites possess large magnetostriction constant [7-9], therefore, they are often used as a ferromagnetic component in composite magnetic dielectrics [10, 11].

In recent years, synthesis of different substances with particles of nanometer sizes with specified properties is one of the leading areas of modern material science [12]. For $CoFe_2O_4$, such parameters as coercive force, saturation magnetization and residual magnetization are closely connected with the size and shape of particles [13], and also with the distribution of cations in their sublattices. Nevertheless, magnetic, dielectric and optical properties of ferrites are very sensitive to the way of their production [14], temperature and sintering conditions.

Nanosize ferrite powders are currently obtained by different ways including co-deposition method, modified oxidation process, hydrolysis method, in a ball mill and other techniques [15-20]. Sol-gel method with participation of auto-combustion (SGA) has a significant advantage over other methods [21], since it is convenient and effective production technique of nanosize powders with reduced energy and material requirements.

As of today, there is no any information about the synthesis of nickel-cobalt ferrites by the SGA method. Therefore, this work is devoted to the synthesis of powders of $Ni_xCo_{1-x}Fe_2O_4$ ferrites, investigation of their structure and study of the optical properties.

2. EXPERIMENTAL

Ferrites of the system $Ni_xCo_{1-x}Fe_2O_4$, where $x = 0.0$, 0.1, 0.2, 0.3, 0.4, and 0.5, were synthesized by the SGA method. The following chemical agents were used during synthesis: nickel nitrate hexahydrate ($Ni(NO_3)_2 \cdot 6H_2O$), cobalt nitrate hexahydrate ($Co(NO_3)_2 \cdot 6H_2O$), iron nitrate nonahydrate ($Fe(NO_3)_3 \cdot 9H_2O$), citric acid ($C_6H_8O_7 \cdot H_2O$) and distilled water. In order to provide high combustion rate, molar ratio 1 : 1 of metal nitrates and citric acid was used. The corresponding amount of each agent was dissolved in 50 ml of water. The pH level of the solution was raised to 7 at constant mixing using 25 % solution of ammonia. Then, at the temperature of 130 °C the solu-

* bushkovavira@gmail.com

tion was dried to its transformation to xerogel. After that, the powders of nickel-cobalt ferrites were obtained due to the auto-combustion process of a dry gel.

The phase composition was controlled by the X-ray analysis which was carried out using the diffractometer DRON-3 with Cu(Kα)-radiation in the range of scanning angles of $20^o \le 2\theta \le 60^o$ with the step of 0.02°.

Determination of the structure-adsorption characteristics of nickel-cobalt powders was performed by the analysis of isotherms of nitrogen sorption at the temperature of 77 K on the automated sorptometer Quantachrome Autosorb (Nova 2200e). The specific surface area of the powders was calculated using the multi-point Brunauer-Emmett-Teller (BET) method at the linear dependence of $1 / [W(P_0 / P) - 1]$ on P / P_0 in the region of adsorption isotherm limited by the range of $P / P_0 = 0.05$-0.35.

The optical absorption spectra are obtained using the spectrophotometer ULAB 102UV in the wavelength range from 200 to 1000 nm with the step of 10 nm.

3. RESULTS AND DISCUSSION

3.1 X-ray study of the synthesized powders

In Fig. 1 we present the cobalt ferrite powder formed during auto-combustion occurring as follows: ammonia water when combined with nitric acid, formed in hydrolysis, forms ammonia nitrate and water.

Decomposition of ammonia nitrate with extraction of the quantity of heat of 38 kJ/mole occurs at the temperature of about 210 °C after completion of the evaporation process of the dispersion medium. Effect of the formation of ferrites from metal oxides also promotes the combustion process.

Organic residues, i.e. citric acid, are burned due to the auto-combustion of xerogel. The power inputs when initiating the auto-combustion reaction are much less than the energy necessary for the long-term high-temperature annealing during ceramic synthesis.

The experimentally X-ray diffraction patterns of the nickel-cobalt ferrite powders after completion of the auto-combustion process are illustrated in Fig. 2. According to the performed analysis, peaks (111), (220), (311), (222), (400), (422), (511) and (440) indicate the presence of the cubic structure of spinel space group $Fd3m$.

The average sizes of the coherent scattering regions (CSR) of Ni-Co ferrite powders are established from the Scherrer formula

$$\langle D \rangle = \frac{0.9\lambda}{\beta \cdot \cos\theta}, \qquad (1)$$

Fig. 1 – Exterior view of the cobalt powder obtained after auto-combustion

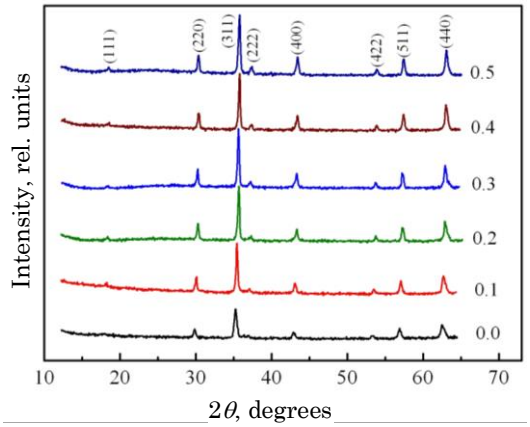

Fig. 2 – Diffraction patterns of the nickel-cobalt powders

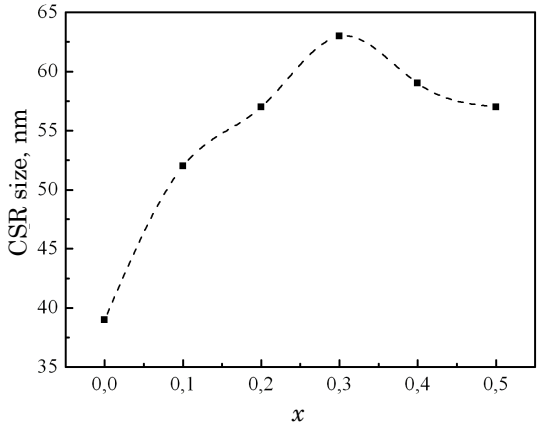

Fig. 3 – Dependence of the CSR size on the composition x

where β is the effective diffraction peak half-width of the X-rays with wavelength λ on angle θ. The calculation results have shown that the average CSR size is in the range of 39-62 nm (Fig. 3).

The values of the lattice constant a and the X-ray density d_x, which are obtained by the following formulas:

$$a = \frac{\lambda}{2\sin\theta}\sqrt{h^2 + k^2 + l^2}, \qquad (2)$$

where l is the wavelength of X-ray radiation, θ are the angles, on which the peaks were observed, h, k, l are the Miller indices;

$$d_x = \frac{8M}{N_A a^3}, \qquad (3)$$

where M is the molar mass of $Ni_xCo_{1-x}Fe_2O_4$ ferrite powders, N_A is the Avogadro number, are shown in Fig. 4.

As seen from Fig. 4, the lattice parameter demonstrates the linear dependence on the concentration of the x component obeying the Vegard law [22]

$$a = \sum_i a_i k_i, \qquad (4)$$

where k_i is the concentration of the i-th component.

Decrease in the lattice parameter with increasing the number of Ni^{2+} cations in the structure of nickel-cobalt ferrites can be explained based on the difference in ionic radiuses. In the studied $Ni_xCo_{1-x}Fe_2O_4$ structure, larger

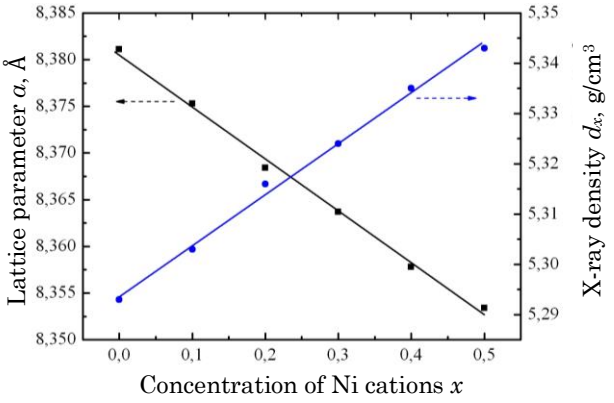

Fig. 4 – Dependence of the lattice parameter and density on the nickel concentration

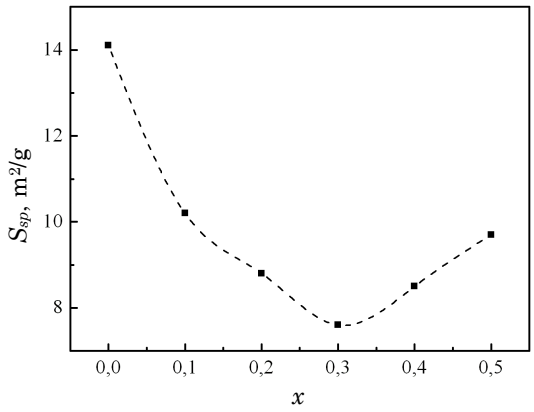

Fig. 5 – Dependence of the specific surface area of the powders on the content of nickel

Co^{2+} ions are substituted by smaller Ni^{2+} ions, therefore, the lattice parameter decreases in this case. A similar trend of change in the parameter a was revealed by the authors of [23]. Lattice parameters of the synthesized powders were found to be slightly lower than their values, which were obtained by the authors of the aforesaid work. As for the X-ray density, its value increases linearly with concentration of nickel, since a nickel atom is heavier than a cobalt atom.

Distribution of cations over spinel sublattices is determined based on the X-ray diffraction patterns by the lattice sites using dependence of the integral intensities of diffraction lines from the positions of atoms in the unit cell and their atomic number. As known [24], relative integral intensities I_{220} / I_{400}, I_{220} / I_{440}, and I_{400} / I_{440} are sensitive to the distribution of cations over spinel sublattices. Change in the concentration of Ni^{2+}, Co^{2+} and Fe^{3+} cations in tetra- and octapositions influences the intensity of X-lines. Ni^{2+} cations prefer B positions, while Co^{2+} and Fe^{3+} cations can occupy A and B positions [25].

The obtained structural formulas for each studied ferrite powder are given in Table 1. It should be noted that $Fe^{3+}(B)/Fe^{3+}(A)$ ratio decreases in connection with the substitution of Co^{2+} cations by Ni^{2+} cations.

Table 1 – Distribution of cations in nickel-cobalt ferrites

Degree of substitution, x	Distribution of cations over spinel sublattices
0.0	$(Co_{0.41}Fe_{0.59})[Co_{0.59}Fe_{1.41}]O_4$
0.1	$(Co_{0.37}Fe_{0.63})[Ni_{0.1}Co_{0.53}Fe_{1.37}]O_4$
0.2	$(Co_{0.34}Fe_{0.66})[Ni_{0.2}Co_{0.46}Fe_{1.34}]O_4$
0.3	$(Co_{0.29}Fe_{0.71})[Ni_{0.3}Co_{0.41}Fe_{1.29}]O_4$
0.4	$(Co_{0.25}Fe_{0.75})[Ni_{0.4}Co_{0.35}Fe_{1.25}]O_4$
0.5	$(Co_{0.21}Fe_{0.79})[Ni_{0.5}Co_{0.29}Fe_{1.21}]O_4$

3.2 Adsorption characteristic of ferrite powders

The values of the specific surface area of the studied system of ferrites using the multi-point BET method is calculated by the experimentally obtained isotherms of nitrogen adsorption [26]. In the process of combustion of a dry gel, gaseous substances are released that leads to the formation of mesopores in the obtained powders. Dependence of the specific surface area of ferrite powders is illustrated in Fig. 5. A powder of the $CoFe_2O_4$ composition has, as it was expected, the largest surface area, since its particles have the smallest sizes, and pores between the particles become an important factor in adsorption of N_2.

We should note that specific surface area of the powders decreases with the addition of Ni^{2+} cations in Ni-Co ferrites to $x = 0.3$, possibly due to the increase in the CSR size, and increases because of their decrease. Such dependence of the specific surface area on the particles size was earlier observed [27].

3.3 Optical properties of nickel-cobalt ferrites

The intensity of light passing through the substance decreases, i.e. light absorption takes place. In general, light absorption can be described from the energy point of view without going into details of the interaction mechanism between light waves with atoms and molecules of the substance, which absorbs light. It is known that when light passes through an absorbing layer of the substance, light intensity I weakens proportionally to the layer thickness d in accordance with the relation called the Buger-Lambert law:

$$I = I_0 e^{-\alpha d}, \qquad (5)$$

where α is the linear light absorption coefficient depending on the type of absorbing substance and wavelength.

If run light with a continuous spectrum through the substance, then, analyzing radiation passed through it, one can determine by the change in the intensity the absorption spectrum of the studied substance, i.e. obtain the dependence of the linear absorption coefficient on the wavelength passing through an absorbing layer of the substance. Therefore, in order to study the influence of the substitution of cobalt ferrite by nickel cations on the semiconductor properties of these ferrites, we have performed the optical investigations by the method of absorption spectrophotometry in ultraviolet, visible and infrared spectral regions.

Dependence of the absorption coefficient on the radiation wave-length is presented in Fig. 6. In general, the interconnection between the semiconductor band gap (E_g), absorption coefficient and radiation frequency (υ) can be expressed by the relation [28]

$$\alpha = \sum_i \alpha_i = \sum_i \frac{A(h\nu - E_{gi})^{m_i}}{h\nu}, \qquad (6)$$

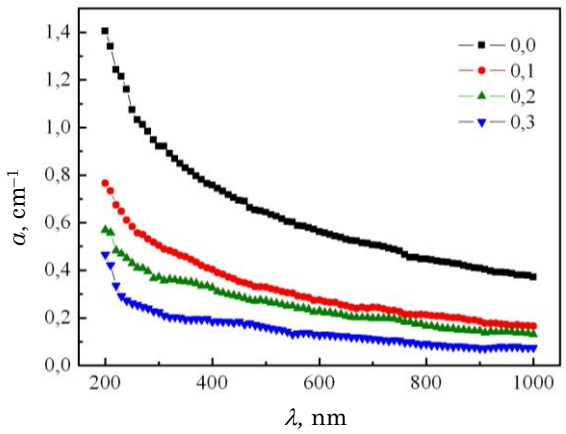

Fig. 6 – Absorption spectra for nickel-cobalt powders

where h is the Planck constant, A is the constant depending on the transition probability, E_{gi} is the energy, m_i is the index characterizing the optical transition nature and equal to 1/2 or 2 for the direct and indirect allowed transitions and 3/2 or 3 for the direct and indirect forbidden transitions, respectively.

For the case, when $E_g = E_{gi}$ and $m = m_i$, equation (6) takes the form

$$\alpha = \frac{A(h\nu - E_g)^m}{h\nu}, \tag{7}$$

whence it follows

$$\alpha h\nu = A(h\nu - E_g)^m. \tag{8}$$

Equation (8) is called the Tautz relation. Let us take logarithms on both sides of the latter relation, and as a result, we obtain

$$\ln(\alpha h\nu) = m\ln(A(h\nu - E_g)). \tag{9}$$

Using the properties of logarithm, equation (9) will have the following form:

$$\ln(\alpha h\nu) = m(\ln A + \ln(h\nu - E_g)). \tag{10}$$

Then, we will differentiate expression (10)

$$d(\ln(\alpha h\nu)) = md(\ln\alpha) + md(\ln(h\nu - E_g)). \tag{11}$$

Since A is the constant, then $d(\ln A) = 0$, and equation (11) will be written as

$$d(\ln(\alpha h\nu)) = \frac{m}{h\nu - E_g}\cdot d(h\nu - E_g), \tag{12}$$

whence based on similar reasons ($d(E_g) = 0$) we obtain

$$\frac{d(\ln(\alpha h\nu))}{d(h\nu)} = \frac{m}{h\nu - E_g}. \tag{13}$$

Taking into account the latter correlation, absorption spectra were plotted in the coordinates $d(\ln(\alpha h\nu))/d(h\nu)$ on $h\nu$ (see Fig. 7).

Estimation of the band gap is performed by the position of the spectral maximum, i.e. the location of the peak corresponding to the transition of electrons from the valence band to the conduction band. For all ferrite powders, the energy value E_0 was approximately equal to 1.67 eV. As for the value of the index m_i, it can be determined by the slope of the linear region of absorption spectra in the coordinates $\ln(\alpha_0 h\nu)$ on $\ln(h\nu - E_0)$ [28].

In Fig. 8 we illustrate the absorption spectra for the nickel-cobalt ferrite in $\ln(\alpha_0 h\nu)$ versus $\ln(h\nu - E_0)$ coordinates. The values of m for all compositions of the studied powders were found to be close to 1/2 that indicates the presence of direct allowed transitions.

Thus, for all investigated ferrite powders, transitions are direct allowed, at that the transition nature does not depend on the degree of substitution of the cobalt ferrite by Ni^{2+} cations.

To obtain the exact value of the optical band gap, the Tautz equation is used. In the case, when $m = 1/2$, expression (8) takes the form

$$\alpha h\nu = A(h\nu - E_g)^{1/2}. \tag{14}$$

We will raise to the square both sides of (14)

$$(\alpha h\nu)^2 = A^2(h\nu - E_g). \tag{15}$$

If $(\alpha h\nu)^2 = 0$, then

$$A^2(h\nu - E_g) = 0. \tag{16}$$

Since A^2 is the constant then we obtain

$$h\nu - E_g = 0, \tag{17}$$

whence it follows

$$E_g = h\nu. \tag{18}$$

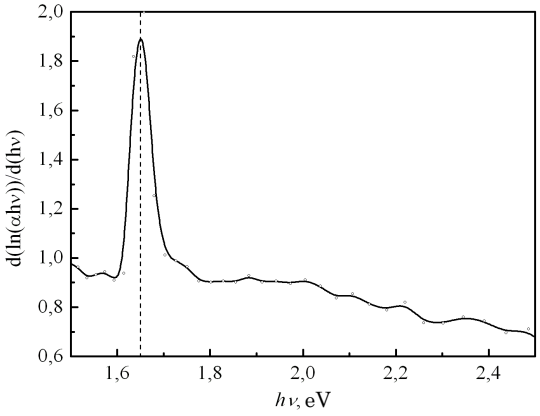

Fig. 7 – Spectrophotometry data in the IR and visible regions for the powder of $CoFe_2O_4$ composition

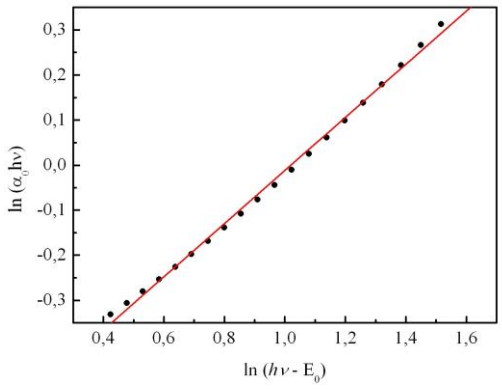

Fig. 8 – Dependence $\ln(\alpha_0 h\nu)$ on $\ln(h\nu - E_0)$ for $Ni_{0,1}Co_{0,9}Fe_2O_4$ powder

Thus, taking into account the above mentioned formulas, we have plotted the spectra for ferrite powders in the coordinates $(\alpha h\nu)^2$ on $h\nu$ (Fig. 9). The optical band gap is determined by the extrapolation of the linear regions of the graphs on the energy axis.

The obtained values of the exponent m and the optical band gap depending on the composition of nickel-cobalt ferrite powders are presented in Table 2.

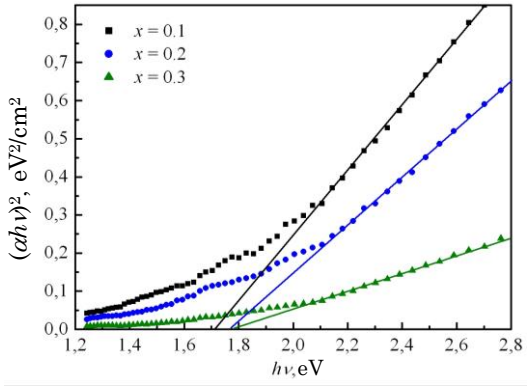

Fig. 9 – Calculation of energies of the direct allowed transitions from the valence band to the conduction band for $Ni_xCo_{1-x}Fe_2O_4$ powders

Table 2 – Optical characteristics of nickel-cobalt ferrites

Composition, x	m	λ, nm	E_g, eV	ε, eV
0.0	0.50	740	1.67	1.75
0.1	0.54	720	1.72	1.32
0.2	0.49	700	1.77	1.23
0.3	0.51	700	1.78	1.41
0.4	0.52	690	1.81	0.94
0.5	0.50	680	1.82	1.10

It is known [29] that the band gap depends on many factors, such as the crystallite size, lattice parameter, and also on the presence of impurities. The obtained value of the band gap increases with increasing concentration of nickel cations in the ferrite composition.

The value of the band gap for a bulk cobalt ferrite is equal to 1.45 eV, and for nickel ferrite – 2.2 eV. In the general case, the values of energies are characterized by the shift towards larger quantities that corresponds to the so-called "blue" shift [30]. This is associated with the size effect, since particles of ferrite powders obtained by the SGA method are much less than the particles of bulk samples.

3.4 Analysis of the "Urbach tail" width

In Fig. 10 we show the theoretical and experimental dependences of $\ln\alpha$ on $h\nu$ for the cobalt ferrite powder. Theoretical dependence of $\ln\alpha$ on $h\nu$ was obtained using the correlation (6) under the condition that $m = 1/2$ and $E_g = 1.67$ eV (Table 2).

Analyzing Fig. 10, it should be noted that the experimentally obtained dependence of the absorption coefficient α agrees well with the theory. An exponential tail called the "Urbach tail" is observed on the experimental dependence of the absorption coefficient with decreasing the photon energy lower than the optical band gap, i.e. at $E_g < 1.67$ eV.

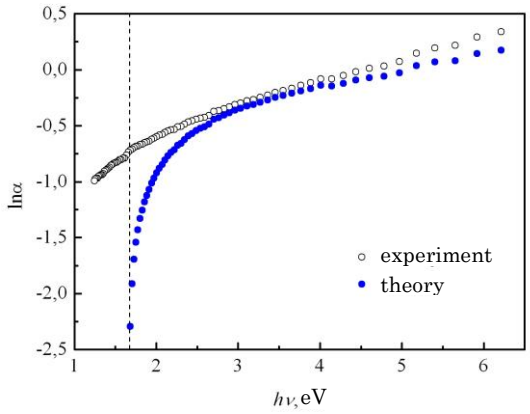

Fig 10 – Dependence of $\ln\alpha$ on $h\nu$ for $CoFe_2O_4$

The "Urbach tail" width ε can be estimated by means of the correlation

$$\alpha = ke^{h\nu/\varepsilon}, \qquad (19)$$

where k is the constant. Taking logarithms on both sides of the latter equation, we obtain

$$\ln\alpha = h\nu/\varepsilon. \qquad (20)$$

Therefore, parameter ε is inversely proportional to the slope of the dependence of $\ln\alpha$ on $h\nu$ (Fig. 11). The values of the "Urbach tail" width are given in Table 2.

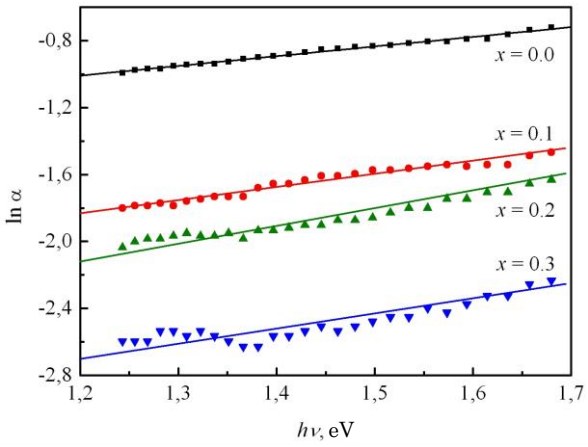

Fig. 11 – Dependence of $\ln\alpha$ on $h\nu$ for ferrite powders

It is known that "Urbach tail" width is responsible for the content of defects in the structure of the material. In the case of crystalline semiconductors, appearance of an exponential tail is a direct result of the induced temperature disorder; moreover, parameter ε reflects the thermal arrangement of the phonon states in the crystal [31]. According to the Cody model [32], the "Urbach tail" width can be described by the relation

$$\varepsilon(T,X) = \frac{k_B\theta}{2\sigma_0}\left(1 + \frac{2}{e^{(\theta/T)-1}} + X\right), \qquad (21)$$

where k_B is the Boltzmann constant, θ is the temperature connected with the Debye temperature by the relation $\theta_D \approx 4\theta/3$, σ_0 is the edge Urbach parameter equal to 1, X is the dimensionless parameter responsible for the struc-

tural disorder. The second term in expression (21) is responsible for the contribution of the electron-phonon and exciton-phonon interactions, and the third term of this equation contains information about deviations of atoms from the perfect lattice structure because of the structural disorder.

In the work, optical absorption spectra for all the studied ferrite powders were collected at room temperature, therefore, different values of the parameter ε for powders of the $Ni_xCo_{1-x}Fe_2O_4$ system are associated with the structural disorder of ferrite particles. Moreover, as a rule, "Urbach tail" width increases with decreasing size of the particles. This is confirmed by the largest value of the parameter $\varepsilon = 1.75$ for $CoFe_2O_4$ powder, whose average CSR size, which is identified with the particle size, is the smallest.

In summary, we can state that exponential tail width or degree of disorder depends on both the composition and the size of nickel-cobalt ferrite powders.

4. CONCLUSIONS

Thus, in this work, we have obtained by the SGA method ferrite powders of the $Ni_xCo_{1-x}Fe_2O_4$ composition and studied their structural characteristics and optical properties. The average CSR size of ferrite powders with the spinel structure is in the range of 39-62 nm.

A monotonic increase in the value of S_{num} is observed with increasing concentration of nickel cations to $x = 0.3$ that is, obviously, the result of the decrease in the linear CSR sizes. We should note that there is a clear correlation between the average CSR sizes and the specific surface area of the powders. Ni^{2+} cations occupy exclusively B sublattice displacing in this case Fe^{3+} cations to the A sublattice that amplifies the superexchange A-B interaction with increasing parameter x.

The presence of direct allowed transition of electrons from the valence band to the conduction band is established for each composition of the powders in the energy spectrum of the studied system. Increase in the optical band gap occurs with increasing number of nickel cations in the $Ni_xCo_{1-x}Fe_2O_4$ system. The obtained energy values (1.67-1.82 eV) in comparison with their values for bulk samples indicate the effect of "blue" shift that is associated with a significant difference in the sizes of ferrite particles.

"Urbach tail" width observed on the experimental dependence of the logarithm of the absorption coefficient on the photon energy is estimated. It is found that the most of structural defects is contained in the cobalt ferrite powder with the smallest particle size.

REFERENCES

1. C. Yang, J. Wu, Y. Hou, *Chem. Commun.* **47**, 5130 (2011).
2. Q. Song, Z.J. Zhang, *J. Am. Chem. Soc.* **126**, 6164 (2004).
3. Y. Qu, H. Yang, N. Yang, Y. Fan, H. Zhu, G. Zou, *Mater. Lett.* **60**, 3548 (2006).
4. M.H. Sousa, F.A. Tourinho, *J. Phys. Chem. B* **105**, 1168 (2001).
5. F. Mazaleyrat, L.K. Varga, *J. Magn. Magn. Mater.* **215**, 253 (2000).
6. Y. Cheng, Yu. Zheng, Yu. Wang, F. Bao, Y. Qin, *J. Solid State Chem.* **178**, 2394 (2005).
7. K. Vasundhara, S.N. Achary, S.K. Deshpande, P.D. Babu, S.S. Meena et al., *J. Appl. Phys.* **113**, 194101 (2013).
8. A.P. Herrera, L. Corrales, E. Chavez, J. Bolivar, O.N.C. Uwakweh, C. Rinaldi, *J. Magn. Magn. Mater.* **328**, 41 (2013).
9. A.S. Ponce, E.F. Chagas, R.J. Prado, C.H.M. Fernandes, A.J. Terezo, E. Baggio-Saitovitch, *J. Magn. Magn. Mater.* **344**, 182 (2013).
10. Xiaobo Wu, Wei Cai, Yi Kan, Pan Yang, Yunfei Liu, Huifeng Bo, Xiaomei Lu, Jinsong Zhu, *Ferroelectrics* **380**, 48 (2009).
11. G.V. Duong, R.S. Turtelli, R. Groessinger, *J. Magn. Magn. Mater.* **322**, 1581 (2010).
12. M.H. Alimuddin, S. Kumar, S.E. Shirsath et al. *Ceram. Int.* **39**, 1807 (2013).
13. J.W.M. Bulte, M. de Cuyper, D. Despres, J.A. Frank, *J. Magn. Magn. Mater.* **194**, 204 (1999).
14. Q. Song, Z.J. Zhang, *J. Phys. Chem. B* **110**, 11205 (2006).
15. Ph. Tailhades, C. Villette, A. Rousset, G.U. Kulkarni, K.P. Kannan, C.N.R. Rao, M. Lenglet, *J. Solid State Chem.* **141**, 56 (1998).
16. Y. Ahn, E.J. Choi, S. Kim, H.N. Ok, *Mater. Lett.* **50**, 47 (2001).
17. N. Hanh, O.K. Quy, N.P. Thuy, L.D. Tung, L. Spinu, *Physica B* **327**, 382 (2003).
18. C.N. Chinnasamy, M. Senoue, B. Jeyadevan, O. Perales-Perez, K. Shinoda, K. Tohji, *J. Colloid Interf. Sci.* **263**, 80 (2003).
19. M.F.F. Lelis, A.O. Porto, C.M. Goncalves, J.D. Fabris, *J. Magn. Magn. Mater.* **278**, 263 (2004).
20. K.P. Chae, J. Lee, H.S. Kweon, Y.B. Lee, *J. Magn. Magn. Mater.* **283**, 103 (2004).
21. A. Kopaev, V. Bushkova, B. Ostafiychuk, *Sol-Gel Synthese und Eigenschaften der weichmagnetischen Nanoferrite und Verbundwerkstoffen. Physik und Technologie der Nanoferrite mit dem Bariumtitanat* (Lap Lambert Academic Publishing: Saarbrücken: 2013).
22. C.G. Whinfrey, D.W. Eckort, A.T. Tauber, *J. Am. Chem. Soc.* **82** No 11, 2695 (1960).
23. S. Singhal, J. Singha, S.K. Barthwalb, K. Chandraa, *J. State Chem.* **178**, 3183 (2005).
24. H. Ohnishi, T. Teranishi, *J. Phys. Soc. Jpn.* **6**, 36 (1969).
25. J.B. Goodenough, A.L. Loeb, *Phys. Rev.* **98**, 391 (1953).
26. S. Brunauer, P.H. Emmett, E. Teller, *J. Am. Chem. Soc.* **60**, 309 (1938).
27. J. Križan, J. Možina, I. Bajsić, M. Mazaj, *Acta. Chim. Slov.* **59** No 1, 163 (2012).
28. S. Chakrabarti, D. Ganguli, S. Chaudhuri, *Physica E* **24**, 333 (2004).
29. Y.S. Wang, P.J. Thomas, P. O'Brien, *J. Phys. Chem. B* **110**, 21412 (2006).
30. N. Kislov, S.S. Srinivasan, Yu. Emirov, E.K. Stefanakos, *Mater. Sci. Eng. B* **153**, 70 (2008).
31. H. Sumi, Y. Toyozawa, *J. Phys. Soc. Jpn.* **31**, 342 (1971).
32. G.D. Cody, T. Tiedje, B. Abeles, B. Brooks, Y. Goldstein, *Phys. Rev. Lett.* **47**, 1480 (1981).